SURFACE CONVECTION: FROM THE SUN TO RED GIANT STARS

L. Piau[1], P. Kervella[2], S. Dib[3] and P. Hauschildt[4]

Abstract. We check how the change in surface conditions between the Sun and red giant branch stars changes the characteristic surface convection length scale to be used in models. We investigate the question in the case of the mixing length theory and of the phenomenology of full spectrum of turbulence. For the observational part, we rely on independent measurements of effective temperatures and interferometric radii of nearby red giants. We find that the local red giant branch cannot be explained taking into account the solar calibrated convective length scale.

Keywords: surface convection, Sun, red giant stars, interferometry

1 Introduction

In low mass stars the effective temperature and the radius estimate the efficiency of surface convection. The Sun and the red giant branch stars (hereafter RGBs) have very different surface conditions. A red giant surface gravity and energy flux are much smaller than the solar ones. The purpose of the work we present is to check how this changes the surface convection efficiency. First we build calibrated solar models using the mixing length theory (hereafter MLT) or the phenomenology of full spectrum of turbulence by Canuto, Goldman & Mazzitelli (1996) (hereafter CGM) for surface convection. Then relying on the same input physics, we build red giant models. The red giant models radii and effective temperatures are compared to an observational sample of 38 objects for which the radii are known directly through interferometry to better than 10 percent. Absolute luminosities and effective temperatures of these objects are also accurately known. In the next section we give the main ingredients of the models affecting the radius and effective temperature and address the solar calibration. In section 3 we describe the RGBs giant sample. Section 4 investigates the changes in characteristic convection length scale from the Sun to RGBs. We conclude in section 5.

2 Models inputs and solar convection length scale

The radii of solar and RGBs models are tuned by the outer thermal gradient. It depends on four ingredients:

1. The opacities. We rely on the OPAL opacities and, below 5600K, on the Ferguson et al. (2005) opacities. The composition is either assumed to be solar with X=0.7392, Z=0.0122 (Asplund et al. 2005) or slightly subsolar at [Fe/H]=-0.17. The metal repartition is always the one of Asplund et al. (2005).

2. Convection efficiency to transport energy. The poor efficiency of outer convection induces the subsurface superadiabatic gradient which in turn sets the entropy of the deep convection zone. A lower entropy level of the deep convection zone means a less dense envelope and thus a wider radius and a lower effective temperature. To model the inefficient convection we use two simplified local treatments of convection: the mixing length theory (Böhm-Vitense 1958) and the full spectrum of turbulence of Canuto, Goldman & Mazzitelli (1996). For both treatments the characteristic convection length scale Λ is assumed to be a constant fraction of the local pressure scale height: $\Lambda = \alpha H_{\mathrm{p}}$.

---

[1] LATMOS, 11 Boulevard d'Alembert, 78280 Guyancourt, France

[2] LESIA, Observatoire de Paris, CNRS UMR 8109, UPMC, Université Paris Diderot, 5 place Jules Janssen, 92195 Meudon, France

[3] Astrophysics Group, Imperial College of Science, Technology and Medicine, London SW7 2AZ, United Kingdom

[4] Hamburger Sternwarte, Gojenbergsweg 112, 21029 Hamburg, Germany

3. Atmospheric effects. At the edge of the star the diffusion approximation does not hold for photons and lines strongly affect the radiative transfer: these effects are expressed by the temperature-optical depth relations that are provided by atmosphere models. We use two series of non-grey atmosphere models as outer boundary conditions. The first series of relations $(T(\tau)^4 = T_{eff}^4 f_{grid}(\tau))$ is computed with the PHOENIX/1D atmosphere code where the convection is handled using the MLT. The second series of temperature-optical depth relations is computed with the Atlas12 atmosphere code (Castelli 2005). We modified Atlas12 to use the CGM prescription. Each type of atmosphere models are used with the corresponding phenomenology of convection in the deeper regions as is necessary for consistency in the models (Montalban et al. 2004).

4. The equation of state influences the radius through the adiabatic exponents. We use the OPAL EoS.

We assume that $L_\odot = 3.846\,10^{33}$ ergs^{-1} and $R_\odot = 6.9599\,10^{10}$ cm and begin the solar evolution on the zero age main sequence. The calibration in luminosity, radius, and metal-to-hydrogen ratio $\frac{Z_{surf}}{X_{surf}}$ are achieved to better than 10^{-4} at the age of 4.6 Ga for both MLT and CGM convection prescriptions. In the MLT framework we obtain $\alpha_{mlt\odot}=1.98$, in the CGM framework we obtain $\alpha_{cgm\odot}=0.77$.

3   The red giant sample

We first queried the CHARM2 catalogue (Richichi et al. 2005) to obtain all direct measurements of giant and subgiant angular diameters up to 2004, with effective temperatures in the range from 5000 K to 5500 K. We then searched the literature for more recent observations, and added the measurement of γ Sge, δ Eri, ξ Hya, and the recent high accuracy CHARA/FLUOR measurements of ϵ Oph and η Ser. The conversion of uniform disk angular diameters to limb-darkened values was done using linear limb-darkening coefficients by Claret et al. (1995), which are based on stellar atmosphere models by Kurucz (1993). Our sample contains 38 giant and subgiant stars with spectral types from G5 to M0. The distances to the selected stars range from 11 to 110 pc. Thanks to this proximity, we neglected the interstellar reddening for the computation of the bolometric luminosity. The accurate parallaxes and interferometric angular radii estimates allow the objects to have a relative uncertainty in the linear radius smaller than 10%. The average metallicity is slightly subsolar [Fe/H] = −0.17 with no object below -0.44 and no object above 0.04 but one exception at 0.13.

4   Red giant branch calibration

We model RGB stars up to 10^3 solar luminosity with exactly the same physics as in the solar models. The microscopic diffusion is accounted for in any model warmer than 5000K following Proffitt & Michaud (1993). This is important in order to obtain correct ages as diffusion speeds up the main sequence evolution. After the first dredge-up though ($T_{eff} < 5000$K) diffusion effects become negligible. Provided the atmosphere boundary models and the opacity tables are unchanged, there are three main models inputs that change the position of the RGB: the mass, the metallicity and the surface convection characteristic length scale. The latter parameter is what we want to constrain. As mentioned above the more efficient the convection, the smaller the radius and the higher the effective temperature at a given luminosity. The metallicity of the sample is known and is therefore no hurdle. The masses of the stars however are not known: unlike RGB stars of a globular or a Galactic cluster, the RGB stars of the sample are field stars that presumably have different masses and ages. Yet it is possible to set an upper limit to the age of local red giants or equivalently a lower limit to their masses. The limit is given by the age of the Galactic disk and the evolutionary timescale of its low mass stars: for objects in the slightly subsolar metallicity range ($−0.25 <$ [Fe/H] $< −0.14$), Liu & Chaboyer (2000) suggest a maximum age of 11.7 ± 1.9 Ga. In this study, we consider models that have reached $10^3 L_\odot$ on the RGB by that age as our RGB stars exhibits [Fe/H] = −0.17 on average. We can set broader upper limits to the local Galactic disk age: it is certainly younger than the Universe 13.7 ± 0.1 Ga (Komatsu et al. 2009). In the next subsections we focus on the lower envelope of the RGB i.e. on these stars with the lower effective temperature or larger radii at a given luminosity (see Figure 1). They are also the oldest and lowest mass stars of the sample.

4.1   Mixing length theory

Figure 2 (left panel) shows the six lower envelope stars of the RGB and features different evolutionary tracks. Let's define $\chi_1^2 = \sum_{i=1}^N (1/N)[(T_{eff}^{mod} - T_{eff}^{obs})/\Delta T_{eff}^{obs}]^2$, where T_{eff}^{obs}, T_{eff}^{mod} and $\Delta T_{eff}^{obs} = 130$K are respectively the
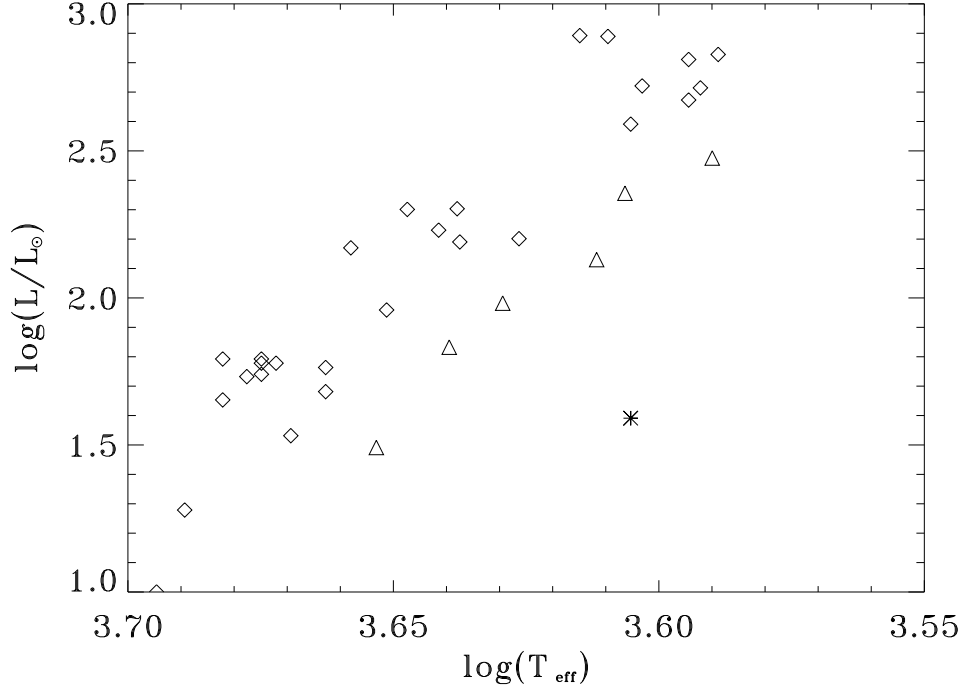
Fig. 1. HR diagram of the RGB stars sample. The triangles define the lower envelope of the RGB in the sense that they show the stars with the lowest effective temperature for a given luminosity.

observed T_{eff} of an object, the T_{eff} of the model having the same luminosity as the object and the uncertainty on the observed T_{eff}. N is the number of objects considered. Figure 2 (left panel) models in solid line, dashed line and dotted line all use the solar calibrated value of $\alpha_{\mathrm{mlt}} = 1.98$. The solid line track corresponds to a $0.95 M_{\odot}$ star reaching $10^3 L_{\odot}$ at ≈ 11.5 Ga. This model has [Fe/H] $= -0.17$ and an helium fraction Y=0.2582. It is clearly too warm to fit the lower envelope of the RGB: $\chi_1^2 = 3.8$. The dashed and dotted lines correspond to less massive and helium poorer stars with $0.9 M_{\odot}$ and Y=0.2482 respectively. The lower mass model is extreme in the sense that it reaches $10^3 L_{\odot}$ at ≈ 13.9 Ga (or $10^2 L_{\odot}$ at ≈ 13.88 Ga), which is older than the current age estimate of the Universe. The helium poor model is also extreme in the sense that its helium fraction nearly is that of Big Bang nucleosynthesis (Coc et al. 2004) and evidently cannot be lowered any further. Both two last models are in slightly better agreement with the data than the former one. Yet they do not provide a good fit to the observations. This demonstrates that mass or helium fraction cannot be changed to improve the agreement to the observations. Models with lower α_{mlt} than the solar value provide much better fits to the data. The three dotted-dashed line is the track of the model with $\alpha_{\mathrm{mlt}} = 1.68$, $0.95 M_{\odot}$, and [Fe/H] $= -0.17$. This model reaches $10^3 L_{\odot}$ at 11.5 Ga and has $\chi_1^2 = 0.16$. The long-dashed line model has $\alpha_{\mathrm{mlt}} = 1.68$, $1.13 M_{\odot}$, and [Fe/H] $= 0$. It reaches $10^3 L_{\odot}$ at 7.5 Ga and has $\chi_1^2 = 0.078$. The analysis in the HR diagram suggests a smaller than solar calibrated characteristic length scale for the MLT.

4.2 Full spectrum of turbulence phenomenology

We will now perform a similar analysis as above but regarding the CGM phenomenology. Furthermore, instead of using T_{eff} we will use the interferometric radii. We therefore do not set ourselves in the HR diagram but in a luminosity vs. square of radius diagram (see Figure 2 right panel). Let's define $\chi_2^2 = \sum_{i=1}^{N}(1/N)[(R_{\mathrm{mod}}^2 - R_{\mathrm{obs}}^2)/\Delta R_{\mathrm{obs}}^2]^2$. Once again N is the number of objects considered. R_{obs}, R_{mod} and ΔR_{obs} are respectively the observed radius of an object, the radius of the model having the same luminosity as the object and the uncertainty on the observed radius. Figure 2 (right panel) shows the nine stars with the largest radii at given luminosities. They were selected by considering the nine largest deviations to a linear fit of the whole sample in the luminosity vs. square radius diagram. The solid line track in Figure 2 (right panel) corresponds to a
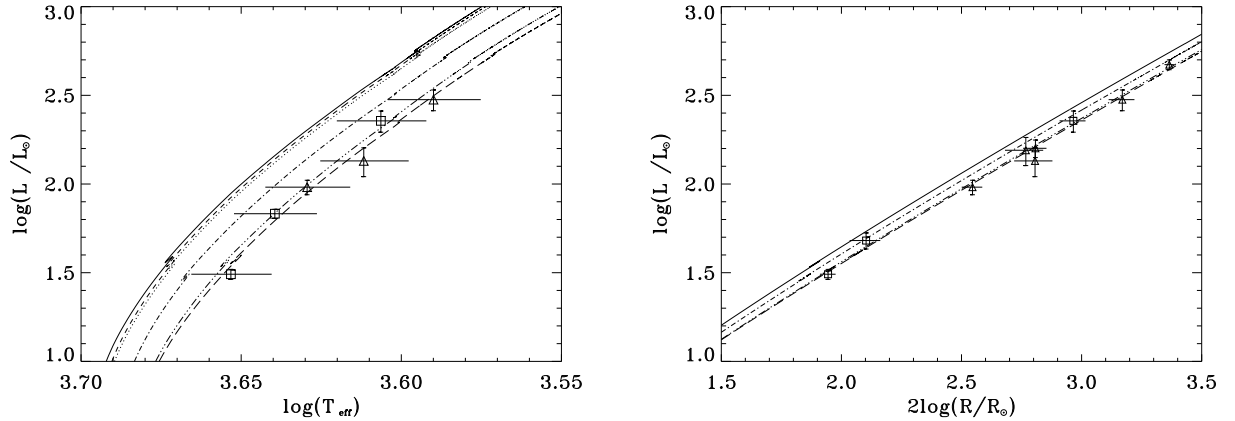
Fig. 2. Left: Position of the six lower envelope stars of the sample with T_{eff} errorbars and various evolutionary tracks computed using the MLT. See text for a description of the corresponding models. **Right:** Position of the nine stars of the sample with largest radii and errorbars. The various evolutionary tracks in overplot were computed using the CGM. See text for a description of the corresponding models.

$0.95 M_\odot$ star reaching $10^3 L_\odot$ at ≈ 11.6 Ga. This model has [Fe/H] = -0.17, an helium fraction Y=0.2582 and the solar-calibrated value $\alpha_{cgm} = 0.77$. This model corresponds to too small radii to fit the lower envelope of the RGB: $\chi_2^2 = 7.2$. As in the case of the MLT, changes in mass and helium fraction are unable to significantly improve the agreement to the data and we will not discuss them. On the opposite if we decrease α_{cgm} down to 0.62 we recover a good agreement to the observations. The three dotted-dashed line is the track of the model with $\alpha_{cgm} = 0.62$, $0.95 M_\odot$, and [Fe/H] = -0.17. This model reaches $10^3 L_\odot$ at 11.8 Ga and has $\chi_2^2 = 0.70$. The long-dashed line model has $\alpha_{mlt} = 0.62$, $1.17 M_\odot$, and [Fe/H] = 0. It reaches $10^3 L_\odot$ at 6.9 Ga and has $\chi_2^2 = 0.40$. The analysis in the luminosity radius diagram suggests a smaller than solar calibrated characteristic length scale for the CGM.

5   Conclusion

We modelled the Sun and local RGB stars in order to check if the change in surface conditions implies a change of the characteristic convection length scale Λ for two local treatments of convection: the MLT and the CGM. In both cases we assume $\Lambda = \alpha H_p$. Therefore we do not consider the original version of the CGM where the characteristic convection length scale is the distance to the boundary with the region stable with respect to convection. At a given absolute luminosity α tunes the position of the RGB in effective temperature and in radius. We have accurate data on absolute luminosities, effective temperatures and radii of all RGB stars we consider. The location of the coolest stars or equivalently the largest radii stars of the sample suggest a decrease in surface characteristic length scale with respect to its solar calibrated value. We have shown the decrease to be required for the MLT in the HR diagram and for the CGM in the luminosity radius diagram. However we could have inverted the diagrams with respect to the convection treatments, the result would have been similar. The reader will find many more details in Piau et al. (2011) where we also specifically address the three RGB stars of the sample with asteroseismic mass estimates. The combination of interferometric and asteroseimic data clearly opens up new perspectives in the understanding of stellar fundamental parameters and how they can be used to constrain stellar physics (Huber et al. 2011).

References

Asplund, M., Grevesse, N., Sauval, J., 2005, ASP Conference Series, Vol XXX.

Böhm-Vitense, E., 1958, Zs. f. Ap., 46, 108

Canuto, V. M., Goldman, I., Mazzitelli, I., 1996, ApJ, 473, 550

Castelli, F., 2005, MSAIt, 8, 25

Claret, A., Diaz-Cordoves, J., Gimenez, A. 1995, A&A Suppl. Ser., 114, 247

Coc, A., Vangioni-Flam, E., Descouvemont, P., Adahchour, A., Angulo, C., 2004, ApJ, 600, 544

Ferguson, J. W., Alexander, D., Allard, F. Barman, T. Bodnarik, J., Hauschildt, P., et al. , 2005, ApJ, 623, 585

Huber, D., et al., 2011, in preparation

Komatsu, E., Dunkley, J., Nolta, M. R., Bennett, C. L., Gold, B., Hinshaw, G., and 13 coauthors, 2009, ApJS, 180, 330

Kurucz, R. L., 1993, CD-ROM 13, Cambridge, SAO

Liu, W. M., Chaboyer, B., ApJ, 2000, 544, 818

Montalban, J., D'Antona, F., Kupka, F., Heiter, U., 2004, A&A, 416, 1081

Piau, L., Kervella, P., Dib, S., Hauschildt, P., 2011, A&A, 526, 100

Proffitt, C. R., Michaud, G., 1993, ASP Conference Series, Vol. 40, 246

Richichi, A., Percheron, I., Khristoforova, M. 2005, A&A, 431, 773